Robust Controller Design of a Dual-Stage Disk Drive Servo System With an Instrumented Suspension

Xinghui Huang, *Student Member, IEEE,* and Roberto Horowitz, *Member, IEEE*

Department of Mechanical Engineering, University of California, Berkeley, CA 94720 USA

This paper proposes a robust track-following controller design method for a dual-stage servo system in magnetic hard disk drives (HDDs). The method formulates the problem of minimizing track misregistration (TMR) in the presence of plant uncertainty and variation as a multiobjective optimization problem. Tracking error minimization is naturally formulated as an H_2 norm minimization problem, while the robust stability issue is addressed by some H_∞ norm bounds. This mixed H_2/H_∞ control problem can then be formulated as a set of linear matrix inequalities (LMIs) and be efficiently solved through convex optimization algorithms. To enhance the system's tracking performance and stability robustness, the method explicitly takes attenuation of airflow-excited suspension vibration into consideration by an inner loop fast rate damping and compensation controller that utilizes the output of a strain gauge sensor on the suspension surface. Analysis and simulation show that a system designed by this method can achieve good tracking performance while still keeping stability robustness to plant variation and high-frequency spillover.

Index Terms—**Hard disk drives, H_2 control, H_∞ control, servo control.**

I. Introduction

ONE of the most important performance measures for hard disk drives (HDDs) is track misregistration (TMR), which is the variance of the deviation of the center of the read/write head from the center of a data track. TMR should be minimized via proper design of the servo system in order to achieve a higher storage capacity in HDDs. As a means of obtaining smaller TMR, dual-stage actuators, which combine a conventional voice coil motor (VCM) and a secondary microactuator (MA) placed close to the head, have been studied intensively [1]–[3]. The design and optimization of track-following controllers for dual-stage actuators have been studied by many researchers over the past years. This work varies from decoupled or sequential single-input-single-output (SISO) classical frequency shaping design techniques, such as the master-slave method [4], the PQ method [5], and the sensitivity decoupling method [6], to those methodologies that explicitly account for the coupling effect between the VCM and MA and that utilize multivariable optimal control design techniques, such as LQG/LTR [7] and μ-synthesis [8]. A general requirement for a disk servo controller is that it should perform well to meet the performance specifications over a huge batch of production drives, while providing internal stability under plant uncertainty and variation from drive to drive. The μ-synthesis technique incorporates stability robustness explicitly in design through some properly modeled uncertainty dynamics or estimated parametric uncertainties. However, μ-synthesis treats tracking error minimization as an H_∞ problem, rather than a more natural and realistic H_2 problem. Other design methodologies can only consider robustness implicitly and partially when optimizing system performance.

In this paper, we propose a design method for dual-stage track-following controllers in hard disk drives. This design method formulates multiple control objectives as a problem of mixed H_2/H_∞ norm constraints that can be expressed as a set of linear matrix inequalities (LMIs). The minimization of TMR is formulated as an H_2 control problem. To retain certain robustness against unmodeled high-frequency dynamics and plant variation, some H_∞ constraints need to be imposed when minimizing the H_2 performance measure of the nominal system. The H_∞ constraints can help to restrict the servo bandwidth within the capability of the system, because the minimization of the H_2 performance measure through sensitivity optimization may result in high bandwidth beyond the working range of the actuators. In the context of disk drive servo design, this design methodology was first applied in [9] for a single-stage system, which contains only a VCM actuator. The design presented in this paper is for a dual-stage servo system with a secondary microelectromechanical systems (MEMS) MA sandwiched between the suspension tip and the slider. Realistic models, such as the VCM, MA, windage, and track runout, are obtained from either experimental tests or finite-element analysis. Furthermore, airflow-excited structural vibration attenuation is explicitly accounted for by an inner loop damping and compensation controller, utilizing a strain sensor signal from the suspension surface. Since the output of the strain sensor can be sampled continuously, it is possible to run the inner loop controller at a higher rate than that of the outer servo loop, which is limited by the sampling rate of the position error signal (PES). Meanwhile, an improved algorithm of norm characterization and controller parametrization has been employed in this design which exhibits less conservativeness and is expected to yield better overall performance [10] over the original algorithm [11].

This paper is organized as follows. Section II describes the dual-stage plant setup and modeling. Section III discusses the design of inner loop vibration damping control. The design of a multiobjective track-following controller is presented in Section IV. Simulation results and detailed analysis are presented in Section V. Section VI concludes the paper.

Digital Object Identifier 10.1109/TMAG.2005.852179

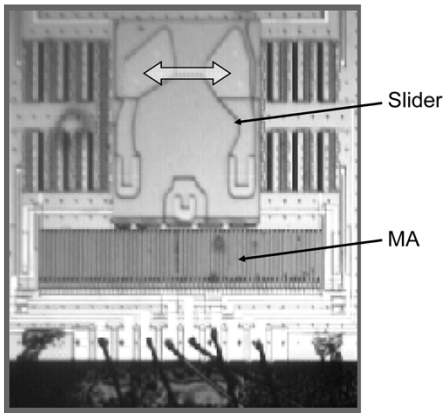

Fig. 1. Translational MEMS MA with a slider mounted on it (courtesy of Kenn Oldham).

II. Dual-Stage Model

The dual-stage servo studied in this paper consists of two actuators: a main VCM actuator and a secondary MEMS MA, which is sandwiched between the gimbal and the slider to provide additional translational motion of the slider relative to the suspension tip, and therefore has the potential for achieving higher servo bandwidth. Fig. 1 shows a photograph of such an MA fabricated in our research group. The block structure of the dual-stage actuator is shown in Fig. 2 and its open-loop frequency responses are shown in Fig. 3. In these figures, u_v and u_m denote the control inputs to the VCM plant G_V and the MA plant G_M respectively; y_v, y_m, and y_h denote the suspension tip position, MA relative motion output or the relative position error signal (RPES), and the read/write head position, respectively. The stain sensor output is denoted y_p, which will be utilized for suspension vibration control. G_C, which derives from the MA dynamics, is the coupling effect from the VCM to the MA. The suspension tip motion y_v is further filtered by G_C before affecting the head position y_h. Since the moving mass of the MA is very small compared to that of the VCM, it is approximated that there is no coupling from the MA to the VCM. So the MA's dynamic response from u_m to y_m is the same as the response from u_m to y_h.

Through finite-element analysis, a VCM model including seven modes is considered. Among them are a pivot friction mode around 60 Hz, a butterfly mode around 7.4 kHz, a suspension sway mode around 10.7 kHz, and four suspension torsion modes around 5.3, 9.1, 13, and 15.2 kHz, respectively. All those suspension flexible modes have relatively small damping ratios around 0.02. To capture the suspension's major resonance modes, a sixth-order model, including the pivot friction mode, the butterfly mode, and the suspension sway mode, is used to approximate the complete model for controller design

$$G_V(s) = \sum_{i=1}^{7} \frac{A_i}{s^2 + 2\zeta_i\omega_i s + \omega_i^2}. \tag{1}$$

Based on experimental testing of the prototype MA, it is modeled to have a moderately damped resonance mode around

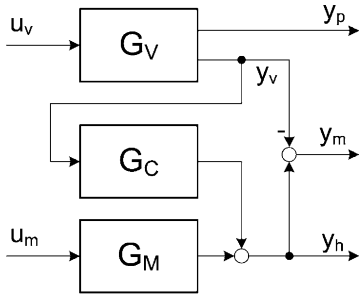

Fig. 2. Block diagram of the dual-stage actuator.

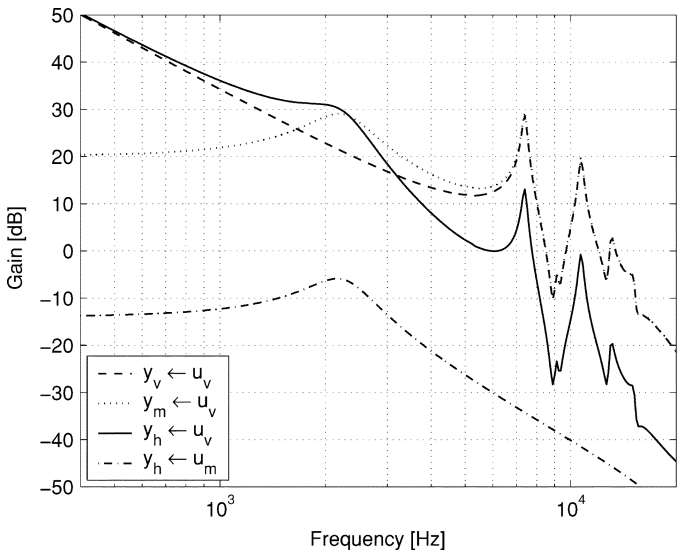

Fig. 3. Frequency responses of the open-loop dual-stage actuator.

2.2 kHz and no other appreciable resonance modes up to 30 kHz. Capacitive sensing has been incorporated into the structure so that the relative motion of the MA, y_m, can be measured

$$G_M(s) = \frac{A_m}{s^2 + 2\zeta_m\omega_m s + \omega_m^2}. \tag{2}$$

The coupling effect G_C is derived from the dynamics of G_M and is expressed as

$$G_C(s) = \frac{2\zeta_m\omega_m s + \omega_m^2}{s^2 + 2\zeta_m\omega_m s + \omega_m^2} \tag{3}$$

with the same notation as in (2).

It is also assumed that a strain sensor is fabricated on the surface of the suspension such that suspension vibration information can be detected for inner loop vibration control [12], [13]. Ideally, one wants the strain sensor to be sensitive to those vibration modes that generate off-track motion of the read/write head, and be insensitive to other irrelevant modes. Similar to the RPES, the strain sensor output, y_p, can also be sampled at a higher rate than that of the PES in order to achieve better vibration control effect. Throughout this paper, both y_p and y_m are assumed to be sampled at 50 kHz, and the PES is sampled at 25 kHz.

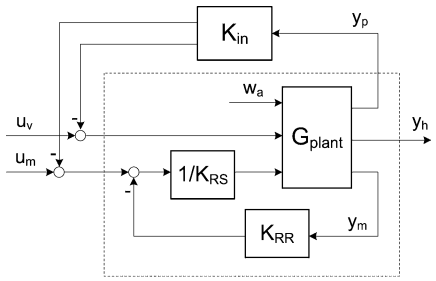

Fig. 4. Block diagram for MA damping and suspension vibration damping and compensation.

III. Design of Inner Loop Vibration Damping and Compensation

With y_m and y_p available as auxiliary information, it is possible to first design some inner loop vibration damping controllers before designing an outer loop tracking controller.

A. MA Damping

The MA's single resonance mode around 2 kHz can be adequately damped by using y_m from the embedded capacitive sensing. It is illustrated in the lower part of Fig. 4. The damping effect yields a well-behaved MA which is critical to the design that follows and its efficacy will be shown in simulations later on. To begin with, first discretize the dual-stage actuator dynamics at 50 kHz with the zeroth-order hold (ZOH), then its discrete-time transfer function becomes

$$G_M(q^{-1}) = \frac{q^{-1}B_o(q^{-1})}{A_o(q^{-1})} \tag{4}$$

where q^{-1} is the one-step delay operator. By pole placement, the damped MA dynamics G_R become

$$G_R(q^{-1}) = \frac{q^{-1}B_o(q^{-1})}{A_R(q^{-1})}. \tag{5}$$

This can be achieved by solving the following Diophantine equation:

$$A_R(q^{-1}) = A_o(q^{-1})K_{RS}(q^{-1}) + q^{-1}B_o(q^{-1})K_{RR}(q^{-1}). \tag{6}$$

The closed-loop polynomial $A_R(q^{-1})$ is chosen by the designer and its roots are poles of the damped MA. Normally the damping ratio for G_R to set to be 1.

B. Suspension Vibration Damping and Compensation

After the minor loop around the MA is closed, the suspension vibration damping and compensation controller, K_{in}, is designed using y_p, which provides vibration information of the suspension. The design of K_{in} is formulated as a standard LQG problem. Consider the discrete-time representation of the plant that already incorporates MA damping, as shown in the outer frame with dashed lines in Fig. 4:

$$\begin{aligned} x(k+1) &= Ax(k) + Bu(k) + B_w w_a(k) \\ y(k) &= Cx(k) + n(k) \end{aligned} \tag{7}$$

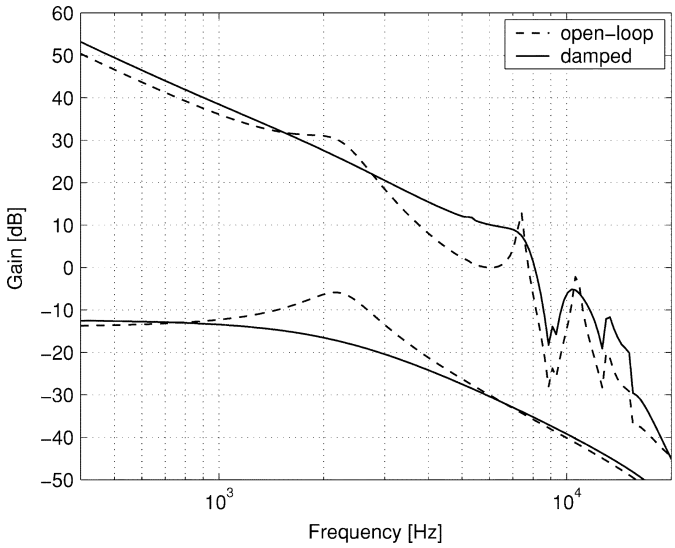

Fig. 5. Plant dynamics with and without vibration damping and compensation.

where $y(k) = [y_h(k)\ y_p(k)]^T$, $u(k) = [u_v(k)\ u_m(k)]^T$, and the airflow turbulence $w_a(k)$ to the suspension and the measurement noise $n(k)$ are assumed to be random sequences with zero mean. The objective of K_{in} is to minimize the cost function

$$J = E\left\{y_h^2(k) + Ru^2(k)\right\} \tag{8}$$

where $E\{\cdot\}$ is the expectation operator, and the control penalty matrix R is given by $R = \text{diag}(r_v, r_m)$ with r_v and r_m the penalties on the control inputs, u_v and u_m, respectively. The controller on the VCM part takes effect by actively *damping* those off-track suspension vibration modes, while the controller on the MA part takes effect by generating additional relative motion to *compensate* for the airflow-excited suspension vibration at the read/write head, since the MA actuation cannot affect the suspension dynamics by assumption. Fig. 5 shows the frequency responses when the MA damping loop and the vibration damping and compensation loop are closed. It is seen that both the MA modes and suspension resonance modes are adequately damped.

IV. Track-Following Control Design

After the two inner loop damping controllers are designed at the high rate, the damped plant is then downsampled to the low rate for the design of the outer loop tracking controller, K_{out}, as shown in Fig. 6. In the figure, G_{in} is the damped plant as shown in Fig. 4. Simulated track runout is generated by the normalized white signal w_r passing through the frequency shaping function G_{RO}. n_1 and n_2 are measurement noises. The objective of tracking control design is to achieve optimal tracking performance while retaining robust stability over some multiplicative uncertainties. This objective is approached through a multiobjective optimization technique via the solution of LMIs and will be detailed in the following subsections.

A. Tracking Error Minimization

The main objective of the HDD servo system is to make the position error signal, PES, as small as possible, in order to

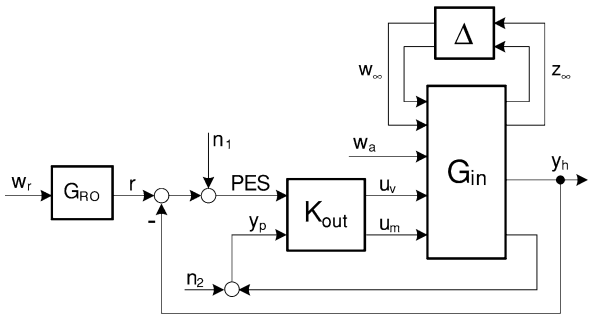

Fig. 6. Block diagram of the outer loop tracking control system.

achieve high areal densities and low-readout error rates. Since the entire system is adequately modeled as a stochastic system, i.e., all external disturbances can be considered as random signals with Gaussian distribution, the tracking performance is normally characterized by the 3σ-value of the PES. When all the disturbance sources are normalized through proper weighting functions, minimizing this root-mean-square (rms) value is then equivalent to minimizing the H_2 norm of the transfer function from those normalized disturbances to the PES, i.e.,

$$\min_{K_{\rm out}} \mathrm{rms}(\mathrm{PES}(t)) \Leftrightarrow \min_{K_{\rm out}} \|G_{z_2 w_2}\|_2 \tag{9}$$

where $z_2 := \mathrm{PES}$ and $w_2 := [w_r w_a n_1 n_2]^T$.

B. Stability Robustness

Stability robustness is an important issue for practical implementation of hard disk servo controllers since there always exist uncertainties and variations in disk drives' plant dynamics. It is infeasible to fine tune controller parameters for each individual disk drive and actual working conditions. Therefore, the designed controller should retain stability over a batch of drives. In other words, it should exhibit stability robustness to those uncertainties and variations. To this end, both qualitative and quantitative information about plant uncertainties need to be known to some extent and be brought into consideration during the design process. There are three main methods of characterizing uncertainties and parameter variations: parametric uncertainty, multiplicative uncertainty and additive uncertainty. To apply the controller synthesis results via LMIs, one needs to address stability robustness by imposing bounds on the H_∞ norms of some appropriately chosen transfer functions. It is therefore necessary to model uncertain dynamics as multiplicative uncertainties. That is, the actual plant dynamics are expressed as

$$G_V(s) = G_{V\mathrm{nom}}(s)(1 + \Delta_V(s) W_V(s)) \tag{10}$$

$$G_M(s) = G_{M\mathrm{nom}}(s)(1 + \Delta_M(s) W_M(s)) \tag{11}$$

where $G_{V\mathrm{nom}}$ and $G_{M\mathrm{nom}}$ denotes the nominal dynamics of the VCM and MA, W_V and W_M are the magnitude bounding functions of the two uncertainties, $\|\Delta_V\|_\infty \le 1$, and $\|\Delta_M\|_\infty \le 1$. Fig. 7 shows the candidate uncertainty bounds used in the simulation.

By assuming multiplicative uncertainties, the uncertain block Δ shown in Fig. 6 becomes a diagonal block with

$$\Delta = \begin{bmatrix} \Delta_V & 0 \\ 0 & \Delta_M \end{bmatrix} \quad \text{and} \quad \sup_\omega \bar{\sigma}(\Delta(j\omega)) \le 1. \tag{12}$$

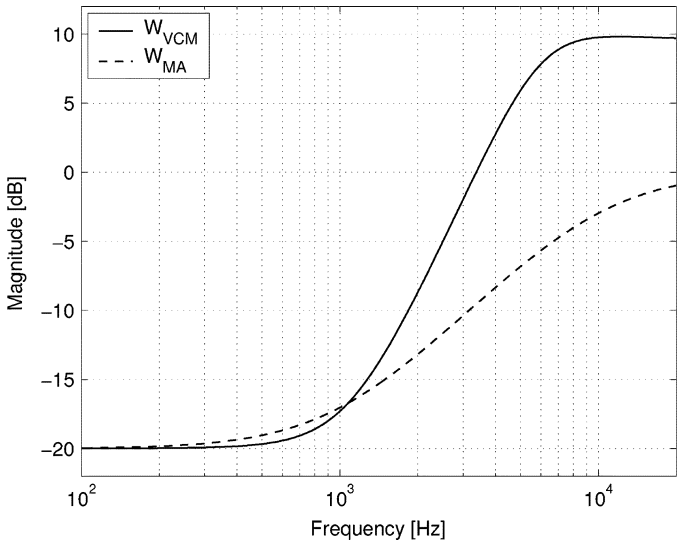

Fig. 7. Uncertainty bounding functions W_V and W_M.

When plant uncertainties are modeled as multiple parametric uncertainties, the system's stability robustness can be more precisely characterized by the structured singular value, $\mu_\Delta(G(j\omega))$, rather than its H_∞ norm, which is normally excessively conservative.

From the μ-theory [14], it is well known that given condition (12), the closed-loop system retains internal stability if and only if

$$\sup_\omega \mu_\Delta(G_{\rm cl}(j\omega)) < 1 \tag{13}$$

where $G_{\rm cl}$ is the closed-loop plant with $K_{\rm out}$ closed around $G_{\rm in}$. This μ-value is in general smaller than $\|G_{\rm cl}\|_\infty$ when Δ is a diagonal, rather than a full complex block. The μ-value and H_∞ norm are equivalent only when the uncertainty block Δ is a full complex matrix. This difference implies that in the dual-stage case, we cannot use the full 2 by 2 Δ block to set the H_∞ norm bound. Instead, an H_∞ norm bound for each uncertain channel (Δ_V or Δ_M) is set first. The two single-channel bounds take on some values strictly less than 1 in order to make sure that when considering both uncertainties, the constraint (13) is still satisfied.

C. Multiobjective Optimization Via LMIS

From the above discussions, we have shown that the controller design of a track-following servo may be cast as an H_2 norm optimization problem with some H_∞ norm constraints, that is, given the general plant, we want to design an output dynamic feedback controller such that

$$K_{\rm out} = \arg\min_{K_{\rm out}} \gamma_2 \tag{14}$$

$$\text{with} \quad \|G_{z_2 w_2}\|_2 < \gamma_2 \tag{15}$$

$$\|G_{w_\infty z_\infty, \Delta_V}\|_\infty < \gamma_V \tag{16}$$

$$\text{and} \quad \|G_{w_\infty z_\infty, \Delta_M}\|_\infty < \gamma_M. \tag{17}$$

Now the problem can be cast as a standard mixed-norm, multiobjective optimization problem. With the aid of the LMI toolbox

in MATLAB [15] and a highly efficient LMI solver SeDuMi [16], this problem can be readily solved and synthesized.

V. Design and Simulation Results

The designed tracking controller is a double-input/double-output (DIDO) dynamic system with the same order as the general plant, which is of order 21. A lower order controller is always preferred in order to reduce the computational time which in turn results in less control delay during implementation. In this design, Hankel model reduction technique [14] was applied to the designed full-order controller and the order of the final controller has been reduced from 21 to 14, without noticeable performance deterioration.

Although the order of the final controller has been greatly reduced, it is still high compared to controllers designed with conventional techniques, such as PID and lead-lag compensator. Care must be taken when implementing the control algorithm. The processor should have enough computation capability so that the computation delay is reduced as much as possible. Our planned experimental testing will be using a DSK6713 board by Texas Instruments, which contains a floating-point 225-MHz DSP and should be adequate to implement the control algorithm. Actually, [9] has successfully implemented a 14-order controller, which is also designed by mixed H_2/H_∞ optimization, in a fixed-point DSP system. In that case, the algorithm was implemented in a cascade form instead of the direct form, so that the sensitivity to the truncation error by fixed-point implementation can be reduced.

A. Controller Dynamics

For illustration purposes, the dynamics of the reduced-order controller from the PES to the VCM control input, u_v, are shown in Fig. 8. Three controllers are considered for comparison: the first controller achieves H_2 norm minimization only, which is equivalent to the standard LQG design; the second one achieves H_2 norm minimization under H_∞ norm constraints, while the third is the reduced-order version of the second one.

From Fig. 8, it is seen that the H_2 controller has multiple peaks and notches, especially in the high-frequency range. These fine features are introduced by mode shapes of the plant dynamics, disturbance shaping functions, and uncertainty weighting functions. These features are expected to shape the controller dynamics in such a way that the optimal tracking performance is achieved, i.e., the rms value of the PES is minimized. However, at this stage, system stability robustness is not guaranteed. When H_∞ bounds are imposed during the design process to guarantee robust stability, those high-frequency peaks corresponding to flexible modes are greatly lowered, in order to attain more stability margin when plant uncertainty becomes large in the high-frequency range.

Fig. 9 shows the Bode plots of the sensitivity transfer functions resulting from the three controllers mentioned above. The bandwidth for these systems is about 3 kHz. The gain and phase margin are about 6.26 dB and 34.4°, respectively. These curves are almost the same except in the low-frequency range. Note that those sensitivity functions do not reflect the vibration attenuation effect in the inner loop, since structural vibrations

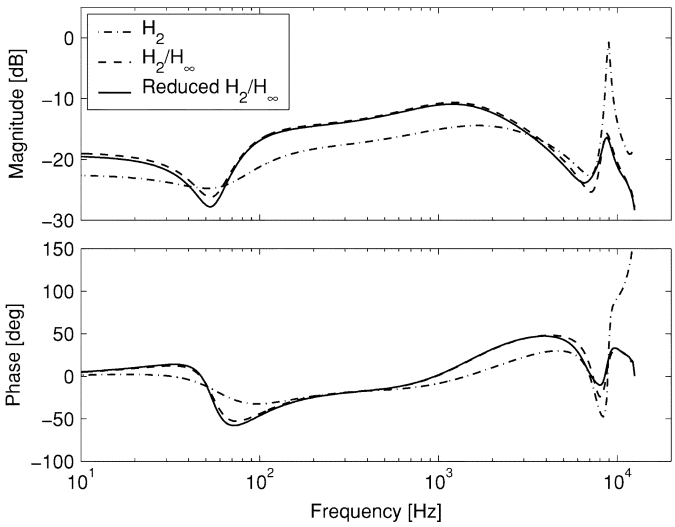

Fig. 8. Bode plots of various controllers.

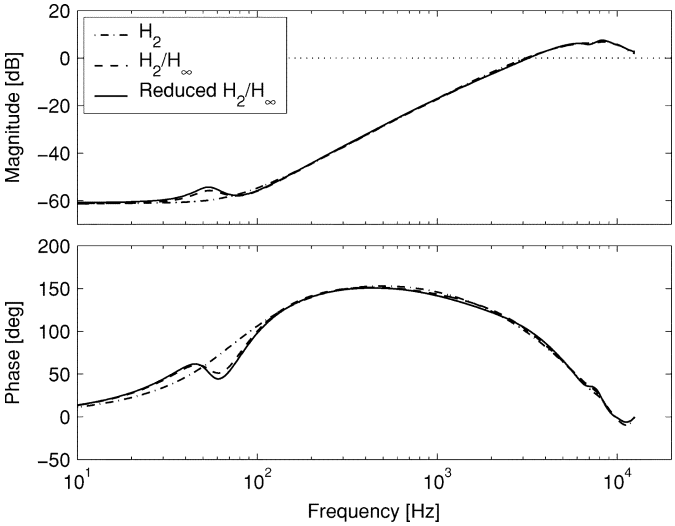

Fig. 9. Bode plots of sensitivity transfer functions resulting from three controller designs.

are mainly excited by airflow turbulence rather than by track runout, and they are already handled by the inner loop vibration damping and compensation controller.

B. Robust Stability Analysis

Stability robustness is an important issue for any control system. In this study, there are at least two aspects that need to be addressed in analyzing the robustness of the proposed control system. First, since the suspension vibration control scheme is a noncollocated control scheme, high-frequency vibration spillover may take place. In other words, the effects on the high-frequency resonance modes not attenuated by the controller could cause instability of the closed-loop system when attenuating the modeled resonance modes. Second, the controller is designed based on the nominal plant. In reality, these parameters vary from drive to drive. What we know is their nominal values and their estimated variation ranges. Therefore, the effect of modal frequency and damping variations on system stability need to be studied. It is noted that the

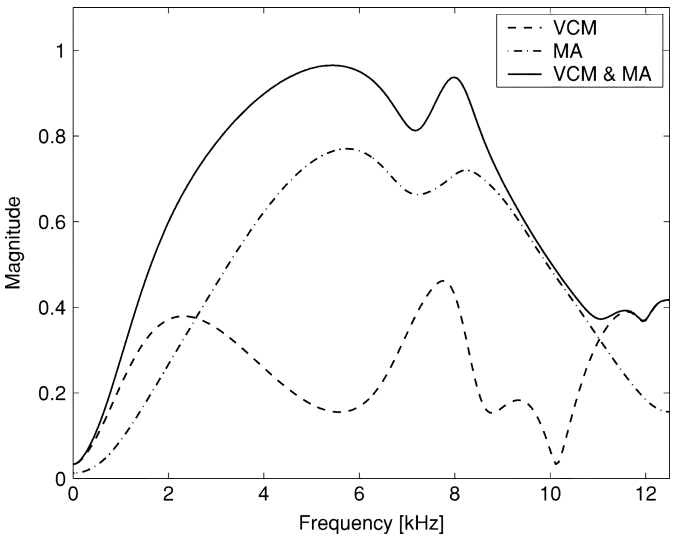

Fig. 10. Stability μ check for different multiplicative uncertainty channels.

reduced order controller will be used throughout the following robust analysis and simulation of the closed-loop system.

As a first step, the μ plots of the closed-loop system for either individual or combined effect of the assumed multiplicative uncertainties, W_V and W_M, are shown in Fig. 10. As shown in the figure, when the two uncertainty channels take effect simultaneously, the resulting μ value (solid curve) is roughly the summation of the μ values when each uncertainty channel takes effect individually. Since the magnitude of the overall μ curve is always less than one, the closed-loop system is robustly stable over the presumed multiplicative uncertainties. The results also explain why a tighter H_∞ bound should be assigned to each uncertainty channel so that the final closed-loop system could still remain stable even when both uncertainty channels take effect simultaneously.

Next, the problems of spillover and parameter variation are studied. Consider a single mode expressed by

$$G(s) = \frac{b_0}{s^2 + a_1 s + a_0} \tag{18}$$

where a_0, a_1, and b_0 are the parameters corresponding to the natural frequency, the damping ratio, and the modal constant of that mode. By assuming a certain percentage of variation for each parameter, a linear fractional transformation (LFT) representation of the variations in these three parameters can easily be derived [14]:

$$y = G_{\text{real}} u = F_U(G_{\text{nom}}, \Delta) u \tag{19}$$

with the diagonal, real-valued uncertainty matrix Δ defined by $\Delta := \text{diag}([\delta_{a_0}\ \delta_{a_1}\ \delta_{b_0}])$. The three normalized real parameters in Δ represent relative variations of the parameters from their nominal values with respective to their variation ranges. With this method, the whole plant, which is a combination of some flexible modes, can be represented in LFTs to incorporate parametric uncertainties.

In this analysis, parameter variations in the uncertain dual-stage actuator model are shown in Table I. The subscript i denotes the seven off-track modes of the suspension. A bigger variation $(\pm 12\%)$ is assumed for the MEMS MA's resonance mode,

TABLE I
RELATIVE VARIATIONS OF MODAL PARAMETERS (i = 1–7)

Parameter	Variation
VCM natural frequency ($\sqrt{a_{i0}}$)	± 8 %
MA natural frequency ($\sqrt{a_0}$)	± 12 %
Damping factor (a_{i1}, a_1)	± 20 %
Modal constant (b_{i0}, b_0)	± 5 %

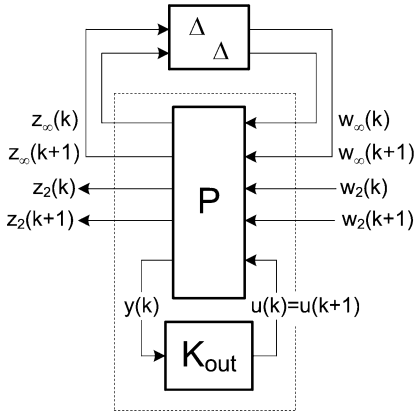

Fig. 11. Plant lifted to retain multirate sensing property.

which is due to lithographic misalignment and variations present in etching processes.

To begin the analysis, the full-order plant model is represented as LFTs to incorporate parametric uncertainties. The two inner loop damping controllers are then closed around the plant to yield a damped plant. This plant is then lifted from 50 to 25 kHz before connecting to the low-order tracking controller. Lifting is an operation to obtain a lower sampling equivalent of a multirate system by grouping the fast sampled signals of the system, such that each group updates at the lower rate. By lifting, the inter-sample behavior, or the high rate updating property of the damped system, is retained when connected to the low-rate outer controller. After the outer controller is closed around the damped plant, μ analysis can be performed on the closed-loop system. Note that, by lifting, both the size of the diagonal Δ block and the multiplicity of each parameter are doubled. The lifting operation is illustrated in Fig. 11. The reader is referred to [14] for details on LFT modeling and μ analysis.

Fig. 12 shows the μ plots for parametric uncertainties. In this figure, the first peak around 2 kHz corresponds to the MA mode variation. The two peaks around 6 and 10 kHz results from the two dominant VCM modes: the butterfly mode and the suspension first sway mode, respectively. And the last peak around 12 kHz is due to the suspension torsion mode around 13 kHz. Obviously this peak reflects the effect of high-frequency spillover. By proper design and parameter selection, all those peaks are kept below 1, implying that the closed-loop system, with y_m and y_p available for damping, remains stable when all modes are included and with parameter variations shown in Table I. We therefore conclude that the system is robust to high-frequency spillover and to some changes in modal frequencies and damping. It is also noted that, when y_m is not used for MA damping, the peak around 2 kHz is much higher with

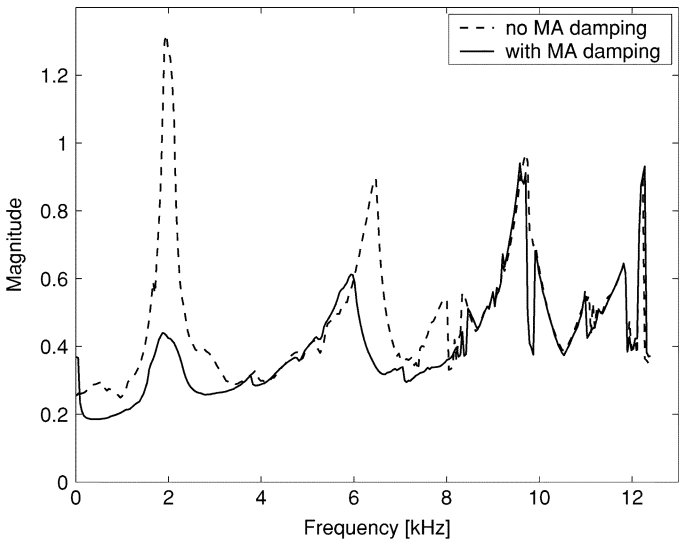

Fig. 12. Stability μ values for parametric uncertainties.

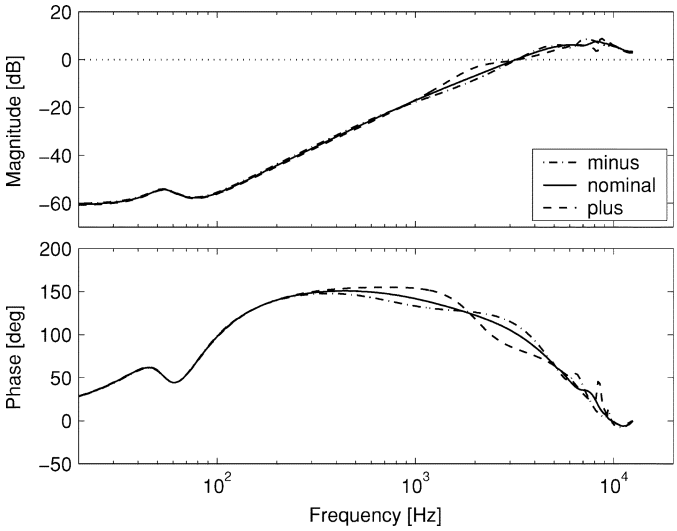

Fig. 13. Sensitivity function responses with parametric uncertainties when y_m is used for damping.

MA parameter variations. This implies that the system is unstable under some variations within the prescribed ranges. A recalculation shows that when the MA damping is not used, the resulted closed-loop system can only withstand a variation of $\pm 8\%$ of the MA natural frequency. This deterioration partially results from the discrepancy between the characterizations of multiplicative and parametric uncertainties, when the first kind of uncertainty is used for design while the second one is used for stability check.

C. Performance Robustness Analysis

Although the stability of the closed-loop system is guaranteed for certain ranges of modal parameter variations, the performance of the system may degrade to become unacceptable before the stability condition is violated. This section investigates the performance under model variations by simulations of the closed-loop system.

Figs. 13 and 14 show the sensitivity function frequency responses with some parameter variations. In the figure, "Minus" denotes the plant in which all modal parameters take on the smallest value within their uncertainty ranges as defined in Table I. For example, the natural frequencies of the VCM all have a -8% change from their nominal values. "Plus" means all parameters take on the largest value within their uncertainty ranges, and "Nominal" denotes the nominal plant. These parameter configurations may not represent the worst cases for the system, but can at least give some insight into the system's performance robustness. From the figure, it is seen that the system without MA damping is more sensitive to MA parameter variation than the system with MA damping. The sensitivity response changes drastically in the range of 2–3 kHz, implying poor performance robustness to MA mode variation. In the high-frequency range, both systems exhibit some minor variation due to suspension mode variations.

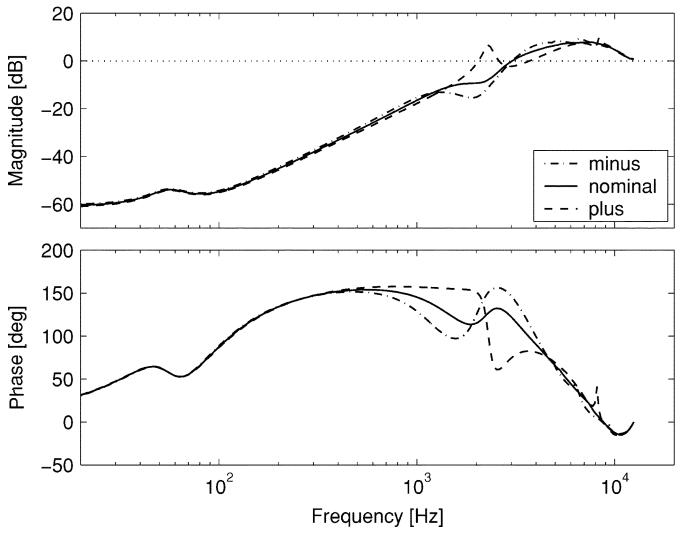

Fig. 14. Sensitivity function responses with parametric uncertainties when y_m is not available.

TABLE II
PERFORMANCE COMPARISON WITH PARAMETER VARIATIONS

	RMS of PES [nm]			Degradation
Configuration	nominal	minus	plus	
with MA damping	3.77	3.92	3.94	5%
no MA damping	4.34	4.51	6.91	53%

Time domain simulations are conducted to check the performance robustness of the two systems with parameter variations. As in the design, the sampling rate of the PES is 25 kHz, while y_p and y_m are sampled at 50 kHz. Simulated track runout, airflow disturbance, and measurement noises are injected to the plant at corresponding locations. Table II shows the rms values of the PES of the two systems with parameter variations. From this table, it can be seen that the system with MA damping is better than the system without MA damping in not only nominal performance but also performance robustness.

VI. CONCLUSION

In this paper, a dual-stage track-following controller is designed based on the mixed H_2/H_∞ optimization method via LMIs. Multirate control is applied to achieve fast-rate feedback

damping of suspension and MA resonance modes. Various system specifications, such as minimization of the rms of PES, and robust stability, are cast into a set of LMIs with controller parametrization. The robust stability criterion for the dual-stage system is adapted such that the multichannel μ constraint can still be satisfied. Analysis and simulation results show that the designed controller can achieve good tracking performance while stability robustness is still maintained under the assumed multiplicative and parametric uncertainties. With MA inner loop damping using its relative motion output, performance robustness is also greatly improved over the case without MA inner loop damping.

Future work involves experimental verification of all those design results. A dual-stage actuator with a MEMS MA has been assembled in our research group, and preliminary testing of the actuator is currently underway. Fabrication of instrumented suspensions are also in progress and they will hopefully be available within a few months. Detailed experiments will be conducted after the dual-stage actuator and the instrumented suspension are assembled.

ACKNOWLEDGMENT

This work was supported by the Information Storage Industry Consortium (INSIC) and the Computer Mechanics Laboratory (CML) of the University of California, Berkeley.

REFERENCES

[1] S. Arya, Y.-S. Lee, W.-M. Lu, M. Staudenmann, and M. Hatchett, "Piezo-based milliactuator on a partially etched suspension," *IEEE Trans. Magn.*, vol. 37, no. 2, pp. 934–939, Mar. 2001.

[2] T. Hirano, L.-S. Fan, W. Lee, J. Hong, W. Imaino, S. Pattanaik, S. Chan, R. Horowitz, S. Aggarwal, and D. Horsley, "High-bandwidth high-accuracy rotary microactuators for magnetic disk drive tracking servos," *IEEE/ASME Trans. Mechatronics*, vol. 3, pp. 156–165, Sep. 1998.

[3] D. Horsley, N. Wongkomet, R. Horowitz, and A. Pisano, "Precision positioning using a micro-fabricated electrostatic actuator," *IEEE Trans. Magn.*, vol. 35, no. 2, pp. 993–999, Mar. 1999.

[4] S. Koganezawa, Y. Uematsu, and T. Yamada, "Dual-stage actuator system for magnetic disk drives using a shear mode piezoelectric microactuator," *IEEE Trans. Magn.*, vol. 35, no. 2, pp. 988–992, Mar. 1999.

[5] S. J. Schroeck and W. C. Messner, "On controller design for linear time-invariant dual-input single-output systems," in *Proc. Amer. Control Conf.*, San Diego, CA, Jun. 1999, pp. 4122–4126.

[6] Y. Li and R. Horowitz, "Mechatronics of electrostatic microactuators for computer disk drive dual-stage servo systems," *IEEE/ASME Trans. Mechatronics*, vol. 6, no. 2, pp. 111–121, Mar. 2001.

[7] X. Hu, W. Guo, T. Huang, and B. M. Chen, "Discrete-time LQG/LTR dual-stage controller design and implementation for high track density hdds," in *Proc. Amer. Control Conf.*, San Diego, CA, Jun. 1999, pp. 4111–4115.

[8] Y. Li and R. Horowitz, "Design and testing of track-following controllers for dual-stage servo systems with PZT actuated suspensions," *Microsyst. Technol.*, vol. 8, pp. 194–205, 2002.

[9] D. H. Shim, H. S. Lee, and L. Guo, "Mixed-objective optimization of track-following controllers using linear matrix inequalities," in *Proc. Amer. Control Conf.*, Denver, CO, Jun. 2003, pp. 4323–4328.

[10] M. C. D. Oliveira, J. C. Geromel, and J. Bernussou, "Extended H_2 and H_∞ norm characterizations and controller parameterizations for discrete-time systems," *Int. J. Control*, vol. 75, no. 9, pp. 666–679, 2002.

[11] C. W. Scherer and S. Weiland, *Lecture Notes DISC Course on LMI in Control*, 2nd ed., 1999.

[12] Y. Huang, M. Banther, P. D. Mathur, and W. Messner, "Design and analysis of a high bandwidth disk drive servo system using an instrumented suspension," *IEEE/ASME Trans. Mechatronics*, vol. 4, no. 2, pp. 196–206, Mar. 1999.

[13] Y. Li, F. Marcassa, R. Horowitz, R. Oboe, and R. Evans, "Track-following control with active vibration damping of a PZT-actuated suspension dual-stage servo system," in *Proc. Amer. Control Conf.*, Denver, CO, Jun. 2003, pp. 2553–2559.

[14] G. J. Balas, J. C. Doyle, K. Glover, A. Packard, and R. Smith, *μ-Analysis and Synthesis Toolbox for Use with MATLAB*. Natick, MA: MUSYN and The MathWorks, 1995.

[15] P. Gahinet, A. Nemirovske, A. J. Laub, and M. Chilali, *LMI Control Toolbox*. Natick, MA: The MathWorks, 1995.

[16] J. F. Sturm, *Using Sedumi 1.05, A MATLAB Toolbox for Optimization Over Symmetric Cones*, 2001.

Manuscript received August 24, 2004; revised May 10, 2005.